Prediction of intestinal absorption and brain penetration of drugs

PhD thesis

Éva Hellinger Pharm.D.

Semmelweis University
Doctoral School of Pharmaceutical Sciences

Supervisor: Dr. Károly Tihanyi Ph.D
Consultant: Dr. Monika Vastag Ph.D

Official reviewers: Prof. Dr. Kornélia Tekes Ph.D.
Dr. Katalin Jemnitz Ph.D.

Head of the Final Exam Committee: Prof. Dr. Tamás Török D.Sc.

Members of the Final Exam Committee:
Prof. Dr. Imre Klebovich D.Sc.
Dr. István Krizbai Ph.D.

Budapest, 2012

1. INTRODUCTION

P-glycoprotein (P-gp, MDR1) is a limiting efflux transporter involved in drug penetration. The P-gp is located on the apical side of polarized cell membranes of both the intestinal mucosa and blood-brain barrier (BBB). P-gp mediated efflux has been recognized as a serious limiting factor in brain entry, and it also influences the intestinal absorption of low permeability or dissolution limited P-gp substrate drugs. Consequently, these drugs have reduced or variable plasma levels and non-linear pharmacokinetics.

The permeability of new chemical entities (NCE) is routinely screened in preclinical drug research. The comparison of various models for the prediction of human absorption as well as brain penetration of NCEs is a prerequisite of successful compound selection.

In the pharmaceutical research Caco-2 is the preferred cell-based model for human drug absorption. However, there is a variable and low expression of P-gp in Caco-2 cultures, which seems to limit its use for screening of P-gp substrates or studying P-gp related interactions. Improved P-gp expression and functionality of Caco-2 cells was set as an objective by several laboratories.

In vitro models of brain penetration that display adequate passive permeability and efflux transporter functionality with good human predictability simultaneously are also much-needed tools in early drug research. The epithelial cell line based surrogate models of BBB penetration can be fast, cheap and easy to handle alternatives of primary brain endothelial-based models in early BBB penetration screening. Highly comparable *in vitro – in vivo* BBB permeability correlations were achievable with epithelial cell MDCK-MDR1 model. Native Caco-2 is also increasingly investigated in comparative studies for BBB permeability prediction too.

For the time being no standard model has yet emerged for the prediction of BBB penetration; there is certainly a lack of comparative data between brain capillary endothelial cell-based models and epithelial-based surrogate models.

2. AIMS

Our aims were:

-To establish a culture with higher and steady P-gp functionality by the modification of Caco-2 cells.

-To examine the effect of sustained vinblastine treatment of Caco-2 cells on the expression and functionality of P-gp (VB-Caco-2).

-To characterize and validate VB-Caco-2 model for long term use for drug penetration screening, P-gp substrate and inhibitor identification in bidirectional transport assay, and in Calcein-AM assay.

-To elucidate the mechanism of vinblastine effect on P-gp level.

-To compare the primary brain capillary endothelial BBB model (EPA) and the epithelial cell-based (Caco-2, VB-Caco-2, MDCK-MDR1) models as possible surrogate BBB models, with special respect to the critical BBB features (presence of discriminative paracellular pathway, BBB-like selective transcellular penetration and expression and function of P-gp).

-To test these models for prediction of *in vivo* BBB penetration.

-To compare a large set of *in vitro* permeability data obtained in parallel with the well accepted surrogate BBB model MDCK-MDR1 and the high P-gp expressing VB-Caco-2 models of drug penetration.

3. METHODS

Cell cultures

Caco-2 cells: Caco-2 cells (HTB-37) at passage 17 were obtained from the ATCC (American Type Culture Collection, Rockville, MD, USA). The cells were routinely cultured and differentiated in standard tissue culture medium consisting of Minimal Essential Medium supplemented with 20% foetal bovine serum, penicillin (100 unit/ml), streptomycin (0.1 mg/ml) and sodium pyruvate (1mM).

VB-Caco-2 cells: VB-Caco-2 cultures were created from Caco-2 cultures by growing cells in 10 nM vinblastine supplemented standard tissue culture medium during subcultivation in flasks and differentiation in Transwell inserts.

For transport assay, Western blot, RT-PCR, CYP activity measurements and electron microscopy the cells were seeded at 5 x 10^5 cells per 1.12 cm^2 density on EC Matrix (ATCC, USA) covered Costar Transwell inserts (polycarbonate, 12 mm diameter, 0.4 μm pore size; Corning Incorporated, Corning, NY, USA) and used for the assays on days 19-21. VB-Caco-2 cultures were studied between passages 48 to 201 and Caco-2 between 35 to 93.

MDCK cells: Parent and MDR1 transfected Madin-Darby canine kidney epithelial cells were obtained from the Netherlands Cancer Institute (Amsterdam, The Netherlands). The cells were cultured in a tissue culture medium consisting of 4.5 g/l glucose containing Dulbecco's Modified Eagle's Medium supplemented with 10% foetal bovine serum, penicillin (50 units) and streptomycin (0.05 mg/ml) all from Gibco. The cells were used for up to 20-30 passages as long as their original properties were preserved. For transport assay and Western blot the cells were seeded at 5 x 10^5 cells per 1.12 cm^2 density on Costar Transwell inserts and used for the assays on days 3-4.

Rat BBB model: Rat brain capillary endothelial cells were used in a triple co-culture model. Primary cultures of brain endothelial cells, astrocytes and pericytes, and construction of the *in vitro* BBB model were prepared by Nakagawa et al. (Nagasaki

University, Japan) and Deli et al. (Biological Research Centre of the Hungarian Academy of Sciences, Szeged, Hungary). Cells were seeded on collagen and fibronectin coated Costar Transwell polycarbonate membranes (12 mm diameter, 3 μm pore size; Corning Incorporated, Corning, NY, USA) for the permeability measurements.

Cell morphology

The morphology of native cells in flasks and toluidine blue stained cells on Transwell inserts was monitored using inverse phase contrast microscopy. Micrographs were taken from cells cultured in T75 flasks. Cells grown on the membrane of the culture inserts were fixed and examined using a Hitachi 7100 transmission electron microscope (Hitachi Ltd., Tokyo, Japan).

Immunostaining

Cells cultured on polyester membrane Transwell-Clear inserts were stained for the junctional proteins β-catenin, ZO-1 and claudin-1, -4 and -5, and monolayers grown on glass coverslips were stained for P-glycoprotein, then were fixed. Cells were blocked with 3% BSA and incubated with primary antibodies (anti-β-catenin, ZO-1, claudin-1, -4, -5 in 1:200 and P-glycoprotein in 1:100 for 1 h 30 min). Incubation with secondary antibody Cy3-labeled anti-rabbit IgG (Sigma–Aldrich) or anti-mouse-IgG-Alexa 488 (Invitrogen), dilution 1: 500, lasted for 1 h.

Real-time PCR

RNA was extracted from cells cultured in flasks and Transwell inserts using RNeasy Mini Kit (Qiagen, Hilden, Germany), following the manufacturer's protocol. The reverse transcription was carried out in a Gene ATAQ Controller thermal cycler (Pharmacia LKB, Uppsala, Sweden). PE Applied Biosystems designed real-time PCR primers for MDR1 and the housekeeping 18S ribosomal RNA and TaqMan universal PCR master mix reagent were used to perform the PCR in 96-well optical reaction plates in an ABI Prism 7000 Sequence Detection System (PE Applied Biosystems).

Western blot

For Western blotting, 25 µg protein samples of cell lysates were loaded on 7.5% Tris-HCl Ready Gels (BioRad Laboratories, Hercules, CA, USA) and blotted onto polyvinylidene difluoride membrane (BioRad Laboratories). Blots were probed with primary mouse anti-P-glycoprotein monoclonal antibody (Clone C219, Calbiochem, La Jolla, CA, USA in a dilution of 1:100 or 1:20), or for loading control with primary rabbit anti-actin polyclonal antibody (1:200, Sigma-Aldrich). Then, secondary antibodies (goat anti-mouse HRP-conjugated IgG; 1:10 000; Calbiochem, for anti-P-gp; or goat anti-rabbit HRP-conjugated IgG antibody 1:3000, Bio-Rad, for anti-actin) were added for 1 hour at room temperature. Chemoluminescence method (SuperSignal West Pico Chemiluminescent Substrate, Thermo scientific Rockford, IL, USA) was applied for detection of P-gp. For loading control, 3,3'-diaminobenzidine (Sigma-Aldrich) was used.

Bidirectional transport assay

The permeability of the test compounds was measured using bidirectional transport assay, in the apical-to-basolateral (A-B) and basolateral-to-apical (B-A) directions at 37 °C with moderate shaking (120 rpm). For highly permeable compounds, the “sink condition” was maintained by transferring the wells with cells to fresh buffer, HBSS-Hepes (Hank's Buffered Salt Solution containing 25 mM Hepes) at given time points (after 15 or 30 or 60 min). For the B-A direction, samples were only taken after the end of the incubation. At least three independent experiments (n=3-3) were performed with triplicate inserts in both directions for reference compounds. Permeability screening was routinely performed under iso pH condition (pH 7.4 $_{A}$-7.4 $_{B}$). Before initiation of the transport studies, TEER (trans epithelial electric resistance) was measured (EVOM-2, WPI Inc, Sarasota, FL). Upon completion of the experiments, epithelial integrity was examined by toluidine blue (1%) staining. Lucifer Yellow (100 µM) and sodium fluorescein (100 µM), markers for the paracellular pathway, were used to verify tight junction integrity.

The concentration of most test compounds in the samples was determined by HPLC with UV-VIS or a fluorescence detector (Merck-Hitachi LaChrom). Apparent permeability (Papp) was calculated with the following equation:

$$\text{Papp} = \frac{(dQ/dt)}{A x C_0}$$

where dQ/dt is the rate of permeability, C_0 is the initial concentration in the donor compartment, and A is the surface area of the filter (1.12 cm^2). The efflux ratio was calculated, as the ratio of $Papp_{B\text{-}A}$ to $Papp_{A\text{-}B}$. A ratio greater than 2.0 was accepted as an indicator of the efflux mechanism involvement. Verapamil HCl or quinidine (100 μM, 30 min preincubation) were used as efflux inhibitors to confirm P-gp activity.

For MDCK-MDR1 cells, the corrected efflux ratio was also calculated (efflux ratio measured in MDCK-MDR1 cells divided by the efflux ratio measured in the parent cells).

Equilibrium dialysis measurements

A 96-well equilibrium dialysis apparatus with 3.5-kDa cut-off membranes was used to determine the free fraction of the drugs in the plasma and brain (HTDialysis LLC, USA). Balb/C mouse blood and brain were obtained fresh on the day of the experiment. Diluted brain homogenate and plasma were spiked with the test compound to give a nominal final concentration of 10 μM of test substance. Dialysis against PBS was carried out in the 96-well equilibrium dialysis plate for 5.5 h at 37°C.

The unbound (free) fraction (fu) for plasma and the apparent fu for brain was determined as the ratio of concentration in buffer to that in plasma or brain. Fu for the brain was calculated with correction for the dilution factor (D):

$$fu = \frac{(1/D)}{\{[1/fu(\text{apparent})]-1\}+1/D}$$

4. RESULTS

Drug penetration model of vinblastine-treated Caco-2 (VB-Caco-2) cultures

The morphological characteristics of VB-Caco-2 cultures showing compact, homogenous monolayers of mostly small diameter cells (**Fig. 1B**) appeared after approx. 6 passages of initiation of 10 nM vinblastine exposure, and were maintained throughout the whole observation period up to 200 passages with continued vinblastine treatment. Contrary to VB-Caco-2, Caco-2 cultures grown in normal tissue culture medium (no vinblastine is added) showed heterogeneous appearance of monolayers consisting of a mixture of patches of small cells among areas covered with relatively large diameter cells (**Fig. 1A**).

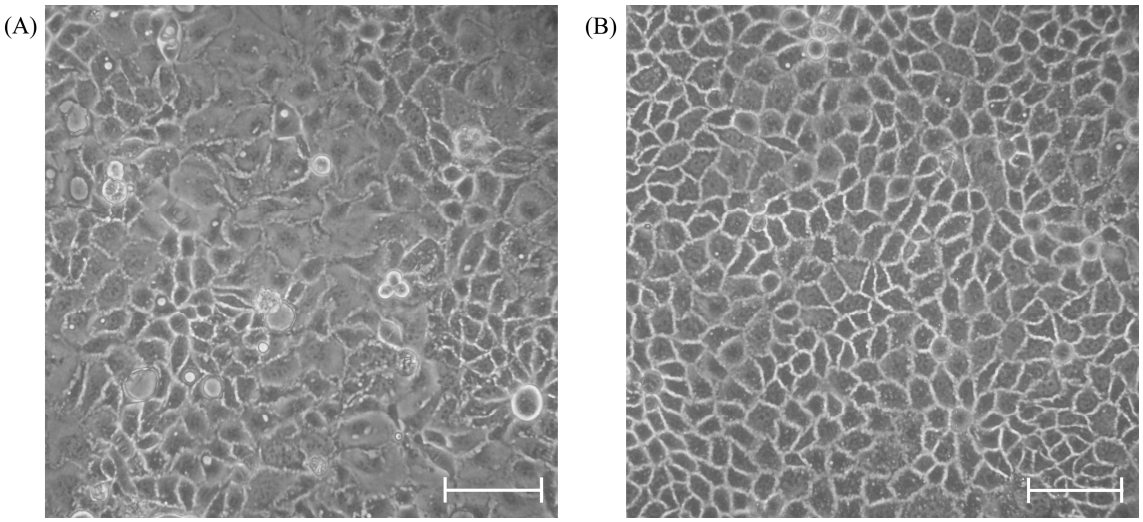

Fig. 1. *Morphology of Caco-2 (A) and VB-Caco-2 (B) monolayers. Cells seeded at a density of 1x 10^6 cells/T-75 flask and cultured for 4 days. Phase contrast images, scale bars: 100 μm.*

P-glycoprotein mRNA and protein levels in VB-Caco-2 and in Caco-2 cultures

In VB-Caco-2 cultures the level of MDR1 mRNA was 2.2 and 4.3 times higher than in differentiated and undifferentiated Caco-2 cultures, respectively. Immunoblots (**Fig. 2**) show most intense expression of P-gp in VB-Caco-2 cultures. In native Caco-2 cultures hardly any detectable level of P-gp protein was observed.

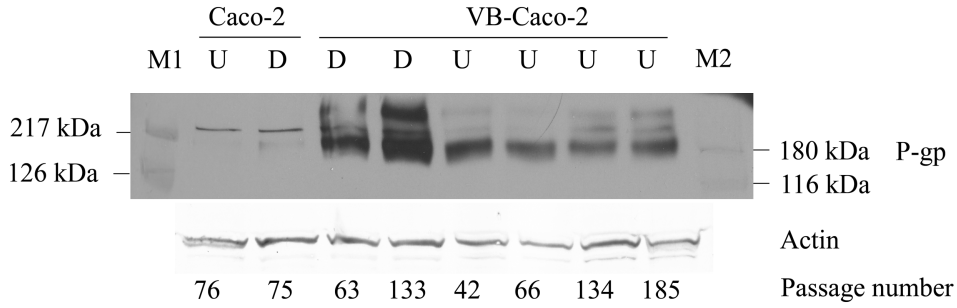

Fig. 2. *Western blot of differentiated (D) and undifferentiated (U) Caco-2 and VB-Caco-2 cell lysates probed for P-gp.* ***M1*** *and* ***M2****: prestained molecular weight markes.*

Functionality of VB-Caco-2 in comparison to Caco-2: passive penetration

The apparent permeability ($Papp_{A-B}$) values obtained for the passively penetrating reference compounds (n=12) correlated strongly ($r^2 = 0.9830$), indicating no substantial difference in the passive drug penetration between the two models. Penetrability of the paracellularly transported Lucifer Yellow and fluorescein sodium was also at the same degree in the two models.

Prediction of human absorption by the models

The apparent permeabilities ($Papp_{A-B}$) of all reference drugs (passively penetrating and efflux mediated) measured in VB-Caco-2 and Caco-2 models were plotted against literature values for HA (human absorption). Two groups of compounds were clearly distinguishable. High permeability compounds with HA of higher than 85% with an apparent permeability of at least 8.5×10^{-6} cm/s or 15.4×10^{-6} cm/s in the VB-Caco-2 or Caco-2 model, respectively; and low permeability compounds with lower than 0.6×10^{-6} cm/s $Papp_{A-B}$ values in the VB-Caco-2 model and with lower than 1.9×10^{-6} cm/s $Papp_{A-B}$ in the Caco-2 model. The higher threshold Papp values with Caco-2 for the two groups were most probably attributable to the lower P-gp sensitivity of those cells (**Fig. 3**).

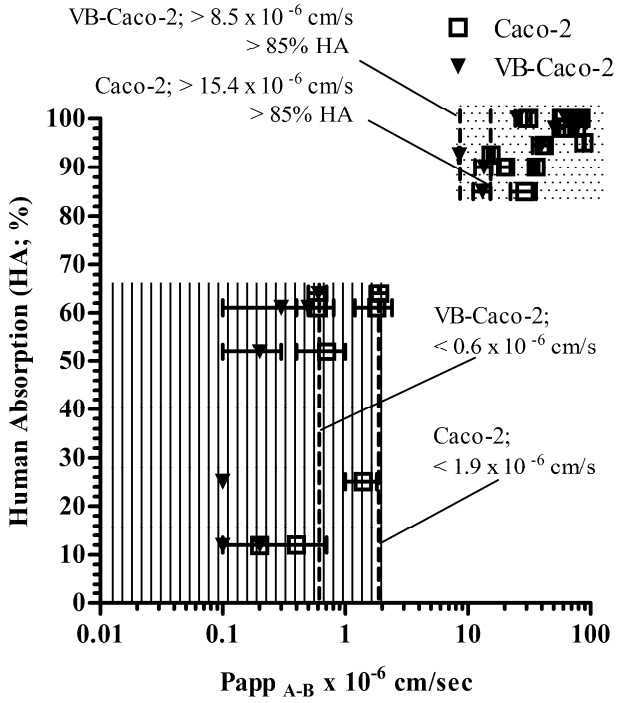

Fig. 3. *The fraction absorbed (HA%, literature data) plotted against apparent permeabilities (Papp$_{A-B}$) of reference drugs in VB-Caco-2 and Caco-2 bidirectional transport assay. The models differentiate two groups of drugs with slightly differing penetrability thresholds (dotted area: high permeability compounds; lined area: low permeability compounds). Bars represent S.D.*

P-gp functionality of VB-Caco-2 compared to Caco-2 in bidirectional transport assay

The VB-Caco-2 assay sensitively detected all the tested P-gp substrates (efflux ratio > 2, n = 11). It correctly classified all low permeability P-gp substrates such as vinblastine, cimetidine, ranitidine, chlorothiazide, atenolol and doxorubicin, and it identified all high permeability P-gp substrates like verapamil, quinidine, dexamethasone, loperamide and labetalol. In contrast to this, the Caco-2 was unable to identify the high permeability reference P-gp substrates, and it also failed to recognize two of the low penetrability references: ranitidine and atenolol. Although other low permeability P-gp substrates such as vinblastine, cimetidine, chlorothiazide and doxorubicin were recognized by Caco-2, the notably higher efflux ratio by the VB-Caco-2 also points to the superior sensitivity of the latter.

The P-gp functionality of VB-Caco-2 was monitored through a broad passage range between 35 and 195. During this interval, each P-gp substrate showed an efflux ratio of higher than 2 at each reading (**Fig. 4**).

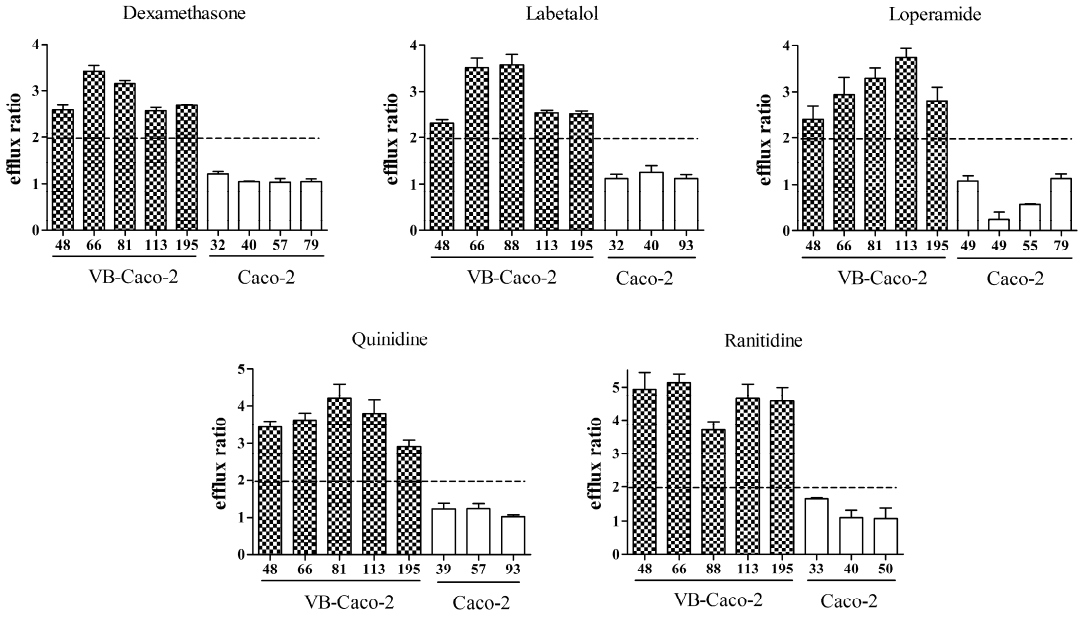

Fig. 4. *Distribution of efflux ratios (mean and S.D. n = 3) of selected P-gp substrates in VB-Caco-2 (filled column) and in Caco-2 cultures (empty column) through a broad passage range. VB-Caco-2 model recognizes with efflux ratio > 2 the known P-gp substrates along the whole observation period. Passage numbers are indicated under the columns.*

The effect of vinblastine withdrawal on P-gp level and functionality in VB-Caco-2 cultures

Vinblastine withdrawal following its sustained presence in VB-Caco-2 cultures (through 70 passages) did not decrease the P-gp protein level or functionality. The protein level of differentiated cultures and bidirectional transport of selected efflux substrates were investigated at 10 and 33 passages after the drug withdrawal.

Screening of NCEs using VB-Caco-2 and Caco-2 bidirectional transport assay

A structurally diverse set of 91 compounds (16 structure families) synthesized in Richter's preclinical research program in four different indication areas underwent permeability screening using both VB-Caco-2 and Caco-2 assays. The results revealed

that 34 out of 91 tested NCEs in VB-Caco-2 assay were P-gp substrates displaying an efflux ratio of > 2, while Caco-2 identified only 8 of them (**Fig. 5**). The Caco-2 failed to identify ~ 76% of compounds. For passively transported compounds (efflux ratio < 2), similar apparent permeability values (r^2 = 0.8706) were obtained in both models in agreement with the observations made on reference drugs.

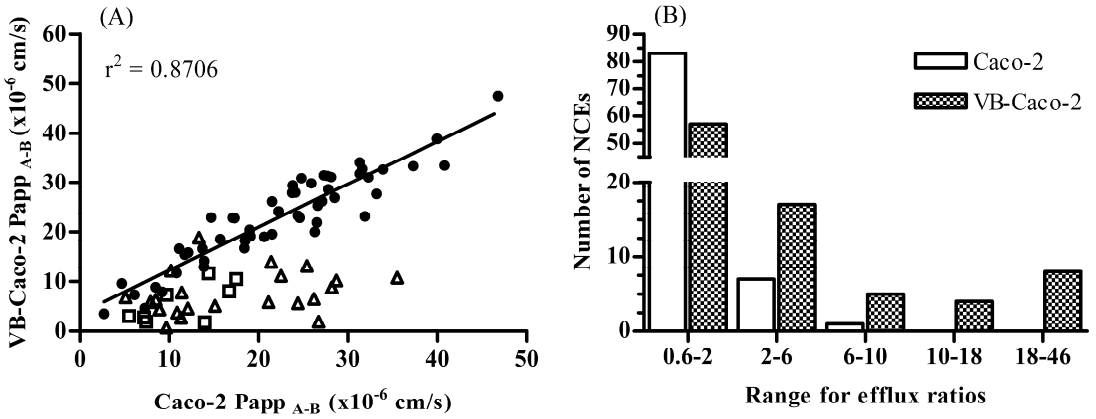

Fig. 5. *Apparent permeabilities (Papp $_{A-B}$) (A) and distribution of efflux ratio values (B) of new chemical entities (NCEs) (n = 91) determined both in VB-Caco-2 and Caco-2 bidirectional permeability assays at iso pH conditions; filled circles: efflux ratio < 2 both in VB-Caco-2 and Caco-2 models (n = 57); open triangles: efflux ratio > 2 only in VB-Caco-2 model (n = 26); open square: efflux ratio > 2 both in VB-Caco-2 and Caco-2 models (n = 8). More assumed P-gp substrates and higher accompanied efflux ratios appeared with the VB-Caco-2 model. The range for efflux of 0.6-2 covers compounds identified as subjects to passive penetration.*

Challenging brain penetration modelling with VB-Caco-2: Comparison of brain capillary endothelial cell-based and epithelial cell-based surrogate BBB penetration models

Morphology: electron microscopy and immunohistochemistry

The height of the brain capillary endothelial cells co-cultured with pericytes and astrocytes was only at about 1.5-2 µm at the perinuclear region (**Fig. 6**). Between the overlapping plasma membranes, the tight junctions, long rows of "kissing points", can be seen. The surface of the endothelial cells is typically smooth but often interrupted by caveolae and caveolae-like invaginations. In the brain capillary endothelial cells, the adherens junctions and desmosomes are in structural unity with the tight junctions.

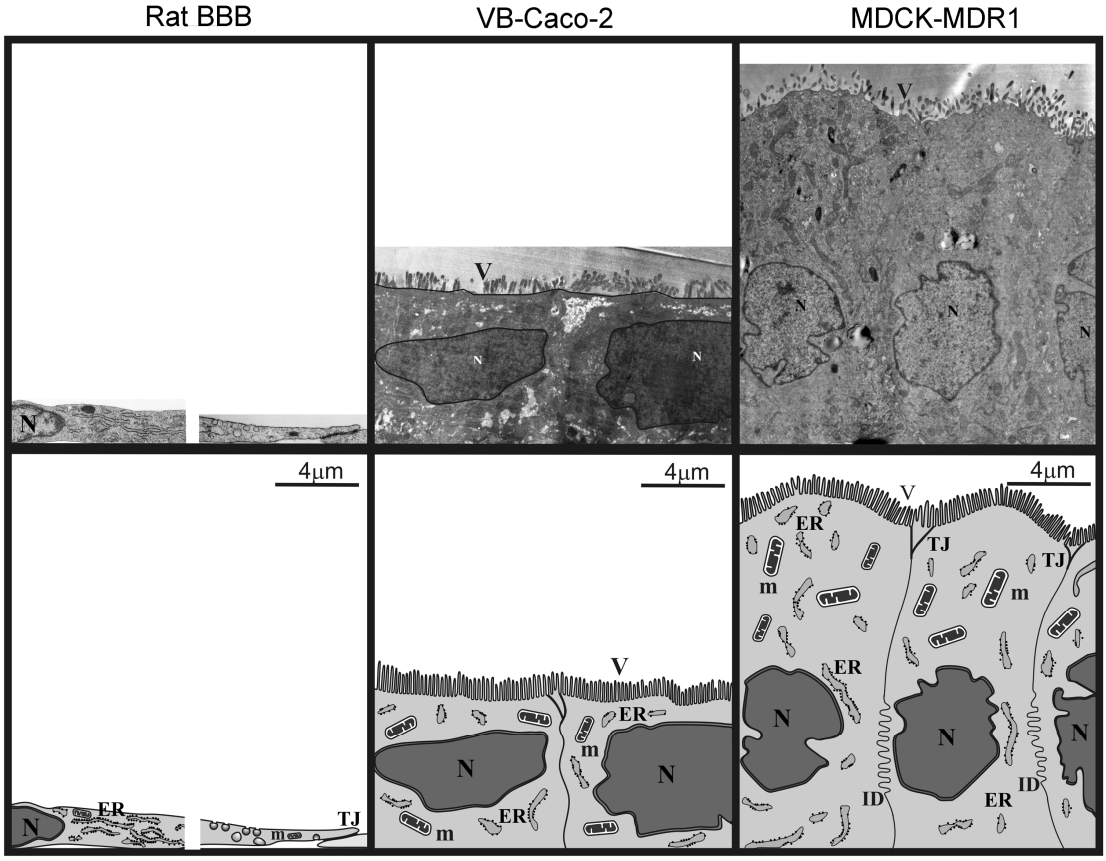

Fig. 6. *Electron micrographs of rat BBB, VB-Caco-2 and MDCK-MDR1 cell cytoarchitecture. ER, endoplasmatic reticulum; ID, interdigitations; m, mitochondrion; N, nucleus; TJ, intercellular tight junctions; V, microvilli.*

Brain endothelial cells stained positively for the endothelial specific claudin-5 but not for the epithelial type claudins (e.g., claudin-1 and -4) and they also yielded positive immunostaining for ZO-1 and β-catenin as well (**Table 1.**). The brain capillary endothelial cells are thin and elongated, and show a swirling pattern in the monolayers.

Table 1. *Summary of the expression of tight junction (TJ) and adherens junction related proteins in rat brain capillary endothelial blood-brain barrier (BBB) and in epithelial models (Caco-2, VB-Caco-2, MDCK-MDR1) using immunostaining.*

Model	β-catenin	ZO-1	Claudin-1	Claudin-4	Claudin-5
Rat BBB	+	+	+/–	–	+
Caco-2	+	+	+	+	–
VB-Caco-2	+	+	+	+	–
MDCK-MDR1	+	+	+	+	–

+: positive staining, –: negative staining

Native Caco-2, VB-Caco-2 and dog kidney epithelial cultures (MDCK, MDCK-MDR1) grow in non-overlapping monolayers and have a cuboidal shape. An obvious morphological difference is that the kidney epithelial cells are usually higher than the colon carcinoma. The apical surface of both cell types is similarly covered with microvilli. Between the adjacent cells, the tight junctions are relatively short (0.3-1 μm), and are positioned apically and well separated from other junctional structures like desmosomes and adherens junctions, so they could be identified as independent structures (**Fig. 6**).

Positive staining for the integral membrane TJ proteins claudin-1 and claudin-4, for the cytoplasmic TJ associated ZO-1 protein and for the adherens junction protein β-catenin was demonstrated in both human colon carcinoma and dog kidney epithelial cells. Epithelial type cells were not stained positively for the endothelial-specific claudin-5 TJ protein. There was a typical cobblestone pattern in both epithelial cultures, but the VB-Caco-2 cultures grow in a lower density than MDCK-MDR1.

P-glycoprotein expression in rat BBB EPA and in epithelial cell lines

Western immunoblots revealed comparably intense staining of P-gp in VB-Caco-2 and MDCK-MDR1 cultures (**Fig. 7**). The P-gp staining in rat brain capillary endothelial cells was less intense and the bands appeared at a lower molecular weight than in human cells. In MDCK and in native Caco-2 cell lysates, the protein level of P-gp was under the detection limit.

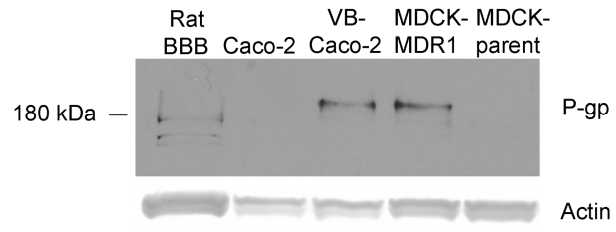

Fig. 7. *Western blot analysis of lysates of rat brain capillary endothelial cells, native Caco-2, VB-Caco-2, MDCK-MDR1 and MDCK-parent cell lines probed for P-glycoprotein (P-gp).*

P-gp immunostaining revealed comparably weaker staining of P-gp for Caco-2, while staining differences were not obvious for the rat BBB, VB-Caco-2 and MDCK-MDR1 cultures.

Comparison of paracellular tightness of the models

The TEER in rat BBB, native Caco-2 and VB-Caco-2 models was well above the critical value (150-200 Ωcm^2), signifying acceptable integrity (**Table 2**). The MDCK(II) and MDCK(II)-MDR1 cultures presented a TEER that was typically below 100 Ωcm^2. The VB-Caco-2 and the MDCK-MDR1 models were the least permeable for fluorescein sodium (NaF), a low molecular weight marker of paracellular integrity, with values of 0.47 x 10^{-6} cm/s and 0.59 x 10^{-6} cm/s, respectively. The rat BBB and native Caco-2 models were looser, as demonstrated by the significantly higher Papp for NaF; (rat BBB: 2.72 x 10^{-6} cm/s; Caco-2: 1.34 x 10^{-6} cm/s; **Table 2**).

Comparison of efflux of P-gp substrate drugs and permeability of mixed mechanism drugs in bidirectional assay

Among the various models, MDCK-MDR1 and VB-Caco-2 identified the highest number of efflux transporter substrates, characterized with an efflux ratio higher than 2, which indicates more sensitive P-gp recognition of these models compared to the others. Accordingly, the MDCK-MDR1 (using a corrected efflux ratio) and the VB-Caco-2 models identified five out of the seven known P-gp substrates tested (**Table 2**, bolded figures). The rat BBB model could only identify digoxin as a P-gp substrate.

Correlation of in vitro and in vivo drug permeability in the models and effect of tissue binding and P-gp functionality

The plasma protein- and brain tissue binding of the reference drugs were measured using equilibrium dialysis. The ratio of fu brain and fu plasma (fu: unbound fraction) values were used for the correction of Papp *in vivo* data (fu uncorrected Papp *in vivo*) that had previously been generated in a mouse brain distribution model.

By *in vitro* equilibrium dialysis antipyrine, caffeine, quinidine, atenolol, digoxin and cimetidine proved to be low plasma protein binding drugs (less than 75% binding), as their fu values were higher than 0.25.

Table 2. *Permeability (Papp) and efflux ratio values of drugs and Trans Epithelial Electric Resistance (TEER, Ωcm2) measured in the rat blood-brain barrier (BBB), native Caco-2, VB-Caco-2, MDCK and MDCK-MDR1 models.*

Compound	Primary transport mech.	Major efflux transporters	Rat BBB			Caco-2			VB-Caco-2			MDCK			MDCK-MDR1			
			$Papp_{A-B}$ x10^{-6} cm/s		efflux ratio	$Papp_{A-B}$ x10^{-6} cm/s		efflux ratio	$Papp_{A-B}$ x10^{-6} cm/s		efflux ratio	$Papp_{A-B}$ x10 -6 cm/sec		efflux ratio	$Papp_{A-B}$ x10^{-6} cm/s		efflux ratio	efflux ratio corrected
			mean	S.D.		mean	S.D.		mean	S.D.		mean	SD		mean	S.D.		
Antipyrine	PT		51.8	1.5	0.88	82.3	3.5	0.80	78.1	2.5	0.97	72.6	2.3	0.98	74.6	3.1	0.96	0.98
Caffeine	PT		64.9	1.9	0.92	84.7	1.0	0.94	85.7	3.0	0.84	79.3	3.2	0.98	78.5	5.6	0.98	1.00
Verapamil	PT/E	P-gp	23.4	2.2	1.36	44.6	8.9	1.33	40.0	7.9	1.60	25.6	10.6	1.59	15.2	0.3	**2.78**	1.75
Indomethacin	PT		33.6	1.3	1.31	50.9	1.4	1.08	50.3	0.5	1.10	47.1	4.4	1.11	45.5	4.3	1.16	1.05
Quinidine	PT/E	P-gp	6.28	0.04	1.93	40.2	3.7	1.06	16.3	3.6	**4.90**	31.8	3.4	1.22	5.19	1.51	**16.4**	**13.5**
Loperamide	PT/E	P-gp	15.6	2.30	1.40	18.1	1.2	1.46	11.5	0.7	**3.13**	9.48	1.03	1.81	4.70	2.67	**17.8**	**9.79**
Atenolol	PP/E	P-gp	1.36	0.20	1.66	0.83	0.19	1.21	0.25	0.09	1.95	0.58	0.20	1.42	0.43	0.14	**2.33**	1.64
Vinblastine	E	P-gp, MRP2	2.42	0.97	0.57	6.97	0.95	**10.5**	0.28	0.07	**270.2**	2.09	0.92	**7.32**	0.21	0.12	**368.5**	**50.5**
Cimetidine	E	P-gp, BCRP	3.86	0.73	0.72	1.97	0.24	**2.23**	0.96	0.56	**3.90**	1.04	0.18	1.32	0.78	0.10	**4.54**	**3.45**
Digoxin	E	P-gp	1.25	0.27	**2.46**	6.50	0.42	**4.72**	0.55	0.17	**65.5**	2.37	0.12	**7.0**	0.57	0.09	**53.1**	**7.56**
Fluorescein-Na	PP		2.72	0.03		1.34	0.29		0.47	0.17		0.65	0.16		0.59	0.06		
			TEER (Ωcm^2), mean ±S.D.															
			548	125		1024	184		2012	347		74	4		84	8		

Compounds were measured at 10 µM, except for sodium fluorescein (100 µM). Bold numbers indicate efflux mechanism (efflux ratio higher than 2). Results for Caco-2, VB-Caco-2, MDCK and MDCK-MDR1 are added as their mean and inter assay S.D. values obtained in at least 3 independent experiments with 3 parallels of identical treatments within assays. For rat BBB model a single experiment (with triplicate inserts) was performed. PT: passive transcellular; PP: passive paracellular; E: Efflux

Verapamil, indomethacin, loperamide and vinblastine appeared to be moderate/high plasma protein binding drugs (binding equal or higher than 90%), with fu of less than or equal to 0.1.

Taking the fu brain values (unbound fraction in brain tissue) determined also with equilibrium dialysis, the fu brain to fu plasma ratios appeared to be close to 1 for caffeine, antipyrine, atenolol, cimetidine and digoxin. The brain tissue binding of verapamil, quinidine and loperamide was slightly higher than their plasma protein binding; therefore, correction with fu brain to fu plasma ratio resulted in a lower *in vivo* Papp values than the uncorrected *in vivo* Papp (2-3-fold shift). The most dramatic shifts in fu corrected Papp *in vivo* appeared for indomethacin (4.9-fold increase) and vinblastine (8-fold decrease). Indomethacin has high plasma protein binding (fu plasma: 0.017) with relative lower brain tissue binding (fu brain: 0.082), but vinblastine has high brain tissue binding (fu brain: 0.013) with relative lower plasma protein (fu plasma: 0.105); therefore, the fu ratios are significantly deviate from one and markedly change the value of the Papp *in vivo*.

Table 3. *The r^2 values of correlations between in vitro permeability (Papp) determined in the different cell-based models of drug permeability and the fu brain/fu plasma ratio corrected or the tissue binding uncorrected in vivo Papp values. BBB, triple co-culture blood-brain barrier model.*

Permeability model	r^2 value	
	in vitro Papp versus fu brain / fu plasma ratio corrected Papp *in vivo*	*in vitro* Papp versus tissue binding un-corrected Papp *in vivo*
Rat BBB	0.7989	0.4391
Caco-2	0.6053	0.4430
VB-Caco-2	0.7206	0.3851
MDCK	0.6809	0.4217
MDCK-MDR1	0.7782	0.3352

The fu corrected or the fu un-corrected Papp *in vivo* data (calculated on the basis of total drug concentrations) of the reference drugs was plotted against the *in vitro* permeability data determined in rat BBB and in native Caco-2, VB-Caco-2, MDCK and MDCK-MDR1 models. When tissue binding uncorrected Papp *in vivo* data was used, no substantial correlation was observed in any of the models *($r^2 < 0.45$)* for the tested

reference compounds (**Table 3**). On the contrary, when the *in vitro* permeabilities were plotted against tissue binding corrected Papp *in vivo* data, a correlation was obtained (r^2=0.7989-0.6053); the goodness of fit was similar in the models (**Table 3**). Those compounds with a significant deviation of the fu brain to fu plasma ratio from 1, such as indomethacin (fu brain to plasma 4.9) and vinblastine (fu brain to plasma 0.12), are outliers if uncorrected data is plotted, whereas corrected values substantially improve the power of correlation.

The results also show the positive effect of P-gp functionality in the models on the goodness of *in vitro – in vivo* correlations. The high and low P-gp functionality counterparts VB-Caco-2 versus Caco-2 and MDCK-MDR1 versus MDCK models clearly point to the trend of better predictivity (higher r^2 value) of the high P-gp functionality model in comparison with its low P-gp counterpart (**Table 3**).

Comparison of high P-gp activity models: VB-Caco-2 versus MDCK-MDR1

In vitro permeability (Papp) was determined for a large set of chemically diverse drugs (n = 59) and NCEs (n = 62) in VB-Caco-2 and the well accepted surrogate BBB model of MDCK-MDR1. A strong correlation was found in terms of the permeability (**Fig. 8**) in the models.

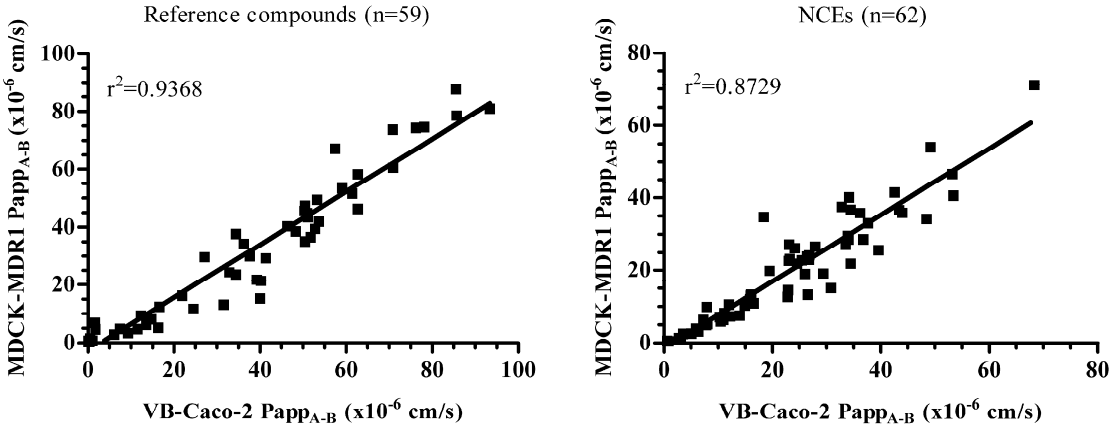

Fig. 8. *Correlation between permeability (Papp) data of reference drugs (n=59) and NCEs (n=62) determined in VB-Caco-2 and in MDCK-MDR1 models.*

5. DISCUSSION

A high P-gp expressing VB-Caco-2 culture was developed via vinblastine treatment of Caco-2 cells and characterized in comparison to Caco-2 culture. The VB-Caco-2 cells show compact, homogenous monolayers, similar passive permeability as Caco-2 model in bidirectional transport assay, but the VB-Caco-2 model is more sensitive in identifying P-gp substrates and could reliably be used with steady P-gp features through long passages. It is suitable for the prediction of drug absorption and examination of P-gp mediated interactions in bidirectional transport assay. We showed that omitting vinblastine from established VB-Caco-2 cultures did not affect either the protein level or the functionality of P-gp, which confirms the selectional mechanism of vinblastine.

Furthermore, comparison of epithelial cell-based models, including the VB-Caco-2 model as possible surrogate BBB models, was performed with the primary brain capillary endothelial BBB model (EPA). Despite the different morphology, epithelial-based models provide integrity that is very much on a par with that of rat BBB model, and the models show similar passive transcellular permeability, which makes them highly comparable to the rat BBB model. While the P-gp functionality of the rat BBB model was low, the VB-Caco-2 and the MDCK-MDR1 models identified the highest number of P-gp substrate drugs. Significant correlation was obtained between the *in vitro* and *in vivo* brain permeability using all models if the *in vivo* values were corrected with the ratio of free fraction of brain and plasma. A strong correlation was found in terms of the permeability in the VB-Caco-2 and the well accepted surrogate BBB model of MDCK-MDR1 for a large set of chemically diverse drugs and NCEs.

In conclusion, the VB-Caco-2 culture provides a reliable tool for the penetration screening of drugs and NCEs. The VB-Caco-2 model with steady P-gp features is suitable for the identification of P-gp substrates with drug-drug interaction potential. The VB-Caco-2 model may provide an alternative of the widely recognized surrogate BBB model MDCK-MDR1 and the more labour-intense and expensive brain capillary endothelial-based BBB model for fast screening of drug candidates for brain permeability.

6. PUBLICATIONS

Publications related to the dissertation:

Hellinger É, Veszelka S, Tóth AE, Walter F, Kittel Á, Bakk ML, Tihanyi K, Háda V, Nakagawa S, Dinh Ha Duy T, Niwa M, Deli MA, Vastag M. (2012) Comparison of brain capillary endothelial cell-based and epithelial (MDCK-MDR1, Caco-2 and VB-Caco-2) cell-based surrogate blood-brain barrier penetration models. Eur J Pharm Biopharm, 82: 340-351. IF_{2010}: 4.304

Vastag M, **Hellinger É**, Bakk ML, Tihanyi K. (2011) Cell-based models of blood-brain barrier penetration. Ther Deliv, 2: 549-553.

Hellinger É, Bakk ML, Pócza P, Tihanyi K, Vastag M. (2010) Drug penetration model of vinblastine-treated Caco-2 cultures. Eur J Pharm Sci, 41: 96-106. IF: 3.291

Book chapter: **Hellinger É**, Vastag M. Intestinal absorption and models of penetration. In: Tihanyi K, Vastag M, (eds.), Solubility, delivery and ADME problems of drugs and drug-candidates. Bentham Science Publishers. 2011: 86-101.

Other publications:

Tihanyi K, Bakk ML, **Hellinger É**, Vastag M. (2010) CYP inhibition-mediated drug-drug interactions. Curr Enzyme Inhib, 6: 130-145.

Boer K, **Hellinger É**, Hellinger A, Pocza P, Pos Z, Demeter P, Baranyai Z, Dede K, Darvas Z. Falus A. (2008) Decreased expression of histamine H1 and H4 receptors suggests disturbance of local regulation in human colorectal tumours by histamine. Eur J Cell Biol, 87: 227-236. IF: 3.955

Jókúti A, **Hellinger É**, Hellinger A, Darvas Z, Falus A, Thurmond RL, Hirschberg A. (2007) Histamine H4 receptor expression is elevated in human nasal polyp tissue. Cell Biol Int, 31: 1367-1370. IF: 1.547